

SUPERCONDUCTIVITY

Field-induced transition within the superconducting state of CeRh₂As₂

S. Khim^{1*}, J. F. Landaeta^{1†}, J. Banda¹, N. Bannor¹, M. Brandó¹, P. M. R. Brydon², D. Hafner¹, R. Küchler¹, R. Cardoso-Gil¹, U. Stockert¹, A. P. Mackenzie¹³, D. F. Agterberg⁴, C. Geibel¹, E. Hassinger^{15*}

Materials with multiple superconducting phases are rare. Here, we report the discovery of two-phase unconventional superconductivity in CeRh₂As₂. Using thermodynamic probes, we establish that the superconducting critical field of its high-field phase is as high as 14 tesla, even though the transition temperature is only 0.26 kelvin. Furthermore, a transition between two different superconducting phases is observed in a *c* axis magnetic field. Local inversion-symmetry breaking at the cerium sites enables Rashba spin-orbit coupling alternating between the cerium sublayers. The staggered Rashba coupling introduces a layer degree of freedom to which the field-induced transition and high critical field seen in experiment are likely related.

The vast majority of unconventional superconductors have simple, single-component phase diagrams. This is surprising because the nature of superfluidity in ³He (*1*) and the fact that degeneracies or near-degeneracies can be expected to result from many of the electronic mechanisms for unconventional superconductivity (*2*) suggest that a number of materials should feature temperature–magnetic field phase diagrams with transitions between different superconducting order parameters within the superconducting state. Until now, however, the only stoichiometric superconductor that has been well established to have such a phase diagram at ambient pressure is UPt₃ (*3–5*).

Here, we report the discovery of this type of phase diagram in the heavy-fermion material CeRh₂As₂. Experimentally, we show that CeRh₂As₂ has extremely high superconducting critical fields of up to 14 T despite a superconducting transition temperature *T*_c of only 0.26 K. Further, when the magnetic field is applied along the crystallographic *c* axis, the superconducting state contains a well-defined internal phase transition at ~4 T, which we identify using several thermodynamic probes. We also suggest that these observations result from physics different from that at play in UPt₃; the key superconducting properties of CeRh₂As₂ are likely a manifestation of local inversion-symmetry breaking and consequent Rashba

spin-orbit coupling in an overall inversion-symmetric crystal structure (*6–13*), a situation for which multiphase superconductivity has been considered in the theoretical literature (*13–15*) but not observed in a material thus far. Combined with distinctive normal-state physics that likely also results from the unusual crystalline environment of Ce, our observations suggest that CeRh₂As₂ will be a benchmark material in which to study the influence of spin-orbit coupling on electronic mechanisms for unconventional superconductivity.

Heavy-fermion superconductivity in CeRh₂As₂

CeRh₂As₂ crystallizes in a centrosymmetric tetragonal CaBe₂Ge₂-type structure (*16*) (Fig. 1A) in which Ce is alternatively stacked with two different Rh-As blocks along the *c* axis; Rh(1) [As(1)] is tetrahedrally coordinated by As(2) [Rh(2)]. There are two Ce atoms per unit cell. The Ce site lacks local inversion symmetry with the polar *C*_{4v} point group. The lattice inversion center lies in the middle of the line connecting the two Ce atoms. We believe that this distinctive structural feature plays a central role in the physics of the superconducting state.

The high-temperature magnetization of single-crystalline CeRh₂As₂ shows paramagnetic Curie-Weiss behavior with an effective moment of 2.56 bohr magnetons (μ_B) per Ce, corresponding to a Ce³⁺ valence state (Fig. 1B). In the whole temperature range, the *ab* plane magnetization is larger than the *c* axis magnetization by up to a factor of two at low temperature. The resistivity $\rho(T)$ depicted in Fig. 1C displays typical heavy-fermion behavior, with increasing resistivity upon decreasing temperature owing to the Kondo effect. At temperatures below a characteristic local maximum at ~40 K, $\rho(T)$ decreases when the heavy quasiparticle bands are formed by hybridization of local 4*f* electrons with the conduction electrons. The large thermopower *S*(*T*) is typical for a Kondo lattice system (Fig. 1D) (*17*). Below 4 K, the specific

heat *C*(*T*)/*T* in Fig. 1E [where the nuclear contribution has been removed (*17*)] increases toward low temperature following a power law with *C*/*T* ∝ *T*^{-0.6}, suggesting non-Fermi liquid behavior and proximity to a quantum critical point (*18*). *C*/*T* reaches a large value of 1 J/mol·K² at *T* = 0.5 K. The Kondo temperature in CeRh₂As₂ is between 20 and 40 K, as estimated from the magnetic entropy *S*_{mag}(*T*) shown in Fig. 1F (*17*). Of note, *S*_{mag} monotonically increases to reach the value *R*ln4 without a plateau at *R*ln2, where *R* is the ideal gas constant, suggesting that the two low-lying doublets of the crystal electric field (CEF) are very close in energy. The estimated separation of ~30 K that is comparable with the Kondo energy could lead to a possible quasi-quartet ground state (*17, 19*). This is a rare example among the tetragonal Ce systems, which usually exhibit a separation of ≥100 K, and again highlights the unusual local Ce environment in CeRh₂As₂.

Below 1 K, two anomalies appear in the specific heat, as shown in Fig. 1, E and G. A small hump is visible at *T*₀ ≈ 0.4 K, where the data depart from the power-law behavior extrapolated from high temperatures, which is depicted by the dashed line. This departure hints at a phase transition to an ordered state. The large jump below 0.3 K results from the transition to a superconducting state involving the *f* electrons. An equal entropy analysis reveals *T*_c = 0.26 K and a height of the jump at *T*_c of $\Delta C|_{T_c} \approx 1$, similar to the Bardeen-Cooper-Schrieffer (BCS) value of 1.4. The residual Sommerfeld coefficient $\gamma = C/T$ for *T* → 0 is possibly a sign of impurities. The diamagnetic drop of the ac susceptibility confirms entry to the superconducting state (Fig. 1H) at a similar *T*_c for the transition midpoint but a slightly higher onset temperature. The drop in resistivity takes place at 0.39 K (Fig. 1I). Although this is close to *T*₀ in zero field, the increase of *T*₀ with in-plane fields (see the specific heat data at 8 and 12 T in Fig. 2A) shows that *T*₀ is not associated with superconductivity but likely signals some other kind of order. The origin of the new order is yet to be determined, but the absence of an anomaly in the magnetic susceptibility at *T*₀ suggests that it might have Ce-4*f* multipolar or nematic character. We ascribe the higher *T*_c in the resistivity and susceptibility to inhomogeneity in the material, as shown in other heavy-fermion systems (*20–22*). These first results indicate that CeRh₂As₂ is a heavy-fermion superconductor where the lowest CEF levels are separated by an energy of similar size as the Kondo temperature, both on the order of 30 K. Just before becoming superconducting at low temperature, the system enters a state of unknown origin. For the remainder of this paper, we focus on the extraordinary superconducting properties of CeRh₂As₂, as

¹Max Planck Institute for Chemical Physics of Solids, 01187 Dresden, Germany. ²Department of Physics and MacDiarmid Institute for Advanced Materials and Nanotechnology, University of Otago, Dunedin 9054, New Zealand. ³Scottish Universities Physics Alliance, School of Physics and Astronomy, University of St Andrews, St Andrews KY16 9SS, UK. ⁴Department of Physics, University of Wisconsin–Milwaukee, Milwaukee, WI 53201, USA. ⁵Physik Department, Technische Universität München, 85748 Garching, Germany. *Corresponding author. Email: elena.hassinger@cpfs.mpg.de (E.H.); seunghyun.khim@cpfs.mpg.de (S.K.) †These authors contributed equally to this work.

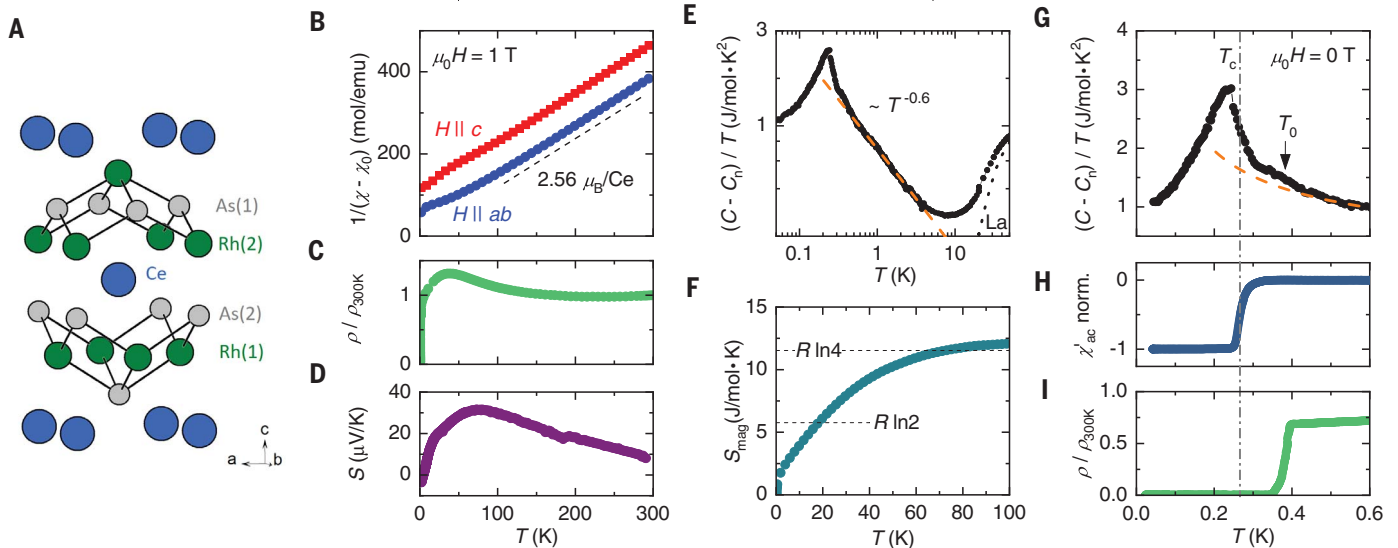


Fig. 1. Crystal structure and heavy-fermion superconductivity in CeRh₂As₂.

The magnetic field $\mu_0 H = 0$ unless indicated otherwise. **(A)** Crystal structure of CeRh₂As₂. **(B)** Inverse magnetic susceptibility $\chi(T)$ [after subtracting a temperature (T)-independent contribution χ_0] in $\mu_0 H = 1$ T applied in the ab plane (blue points) and along the c axis (red points). The dashed line denotes the linear slope for the effective moment of Ce³⁺. emu, electromagnetic unit. **(C)** The resistivity $\rho(T)$ with the current in the ab plane, normalized at 300 K. **(D)** The thermopower $S(T)$ with a temperature gradient in the ab plane. **(E)** The

specific heat $(C - C_n)/T(T)$. A nuclear contribution C_n was subtracted at low T (17). The dotted line presents the LaRh₂As₂ data used to subtract the phonon contribution. The dashed line represents the power-law T dependence. **(F)** The Ce magnetic entropy $S_{\text{mag}}(T)$. **(G–I)** Experimental signatures at the superconducting transition T_c and at the transition T_0 ; see the text for details. **(G)** Specific heat $(C - C_n)/T(T)$ including the same dashed line as in **(E)** and transition temperatures as indicated. **(H)** Normalized ac susceptibility χ'_{ac} . **(I)** The normalized electrical resistivity $\rho(T)$.

established experimentally using magnetic susceptibility and thermodynamic probes.

Figure 2 shows the temperature dependence of the specific heat C/T (panels A and B) and the magnetic ac susceptibility χ'_{ac} (panels C and D) for different magnetic fields between 0 and 14 T for $H||ab$ (panels A and C) and $H||c$ (panels B and D). T_c is defined via the equal entropy method in C/T and at the onset of the susceptibility transition (chosen arbitrarily by the temperature where χ'_{ac} has dropped to the value indicated by the dashed line); T_c shifts down with increasing field. In χ'_{ac} , we observe a relatively strong shift of T_c in a field of 0.1 T that is absent in the specific heat, which is again a sign of nonbulk superconductivity (fig. S7) (17). Increasing the field further reduces T_c more slowly. The superconducting transition is completely suppressed down to 0.05 K at magnetic fields of 14 T for $H||c$ and 2 T for $H||ab$. We note that, especially for $H||c$, these are huge critical fields for a superconductor with a T_c of only 0.26 K. For $H||c$, the temperature sweeps (Fig. 2, B and D) imply a kink in the $T_c(H)$ curve where, above 4 T, the decrease of T_c is slower than below this field.

Two superconducting phases

A pronounced kink in $T_c(H)$ is suggestive of the existence of two superconducting phases. This is confirmed by field sweeps of the ac susceptibility and two separate thermody-

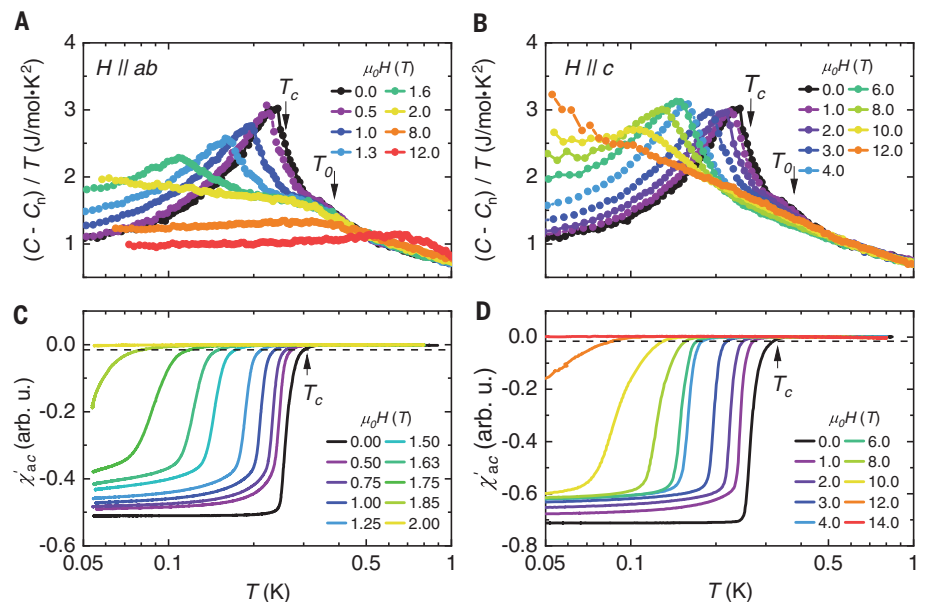


Fig. 2. Evolution of the superconducting transition with magnetic fields. Temperature dependence of the specific heat C/T **(A)** and the real part of the ac susceptibility χ'_{ac} **(C)**, respectively, for $H||ab$. **(B)** and **(D)** same for $H||c$. The dashed lines in **(C)** and **(D)** indicate the value of χ'_{ac} where the onset temperature T_c is defined. arb. u., arbitrary units.

namic probes, magnetization and magnetostriction (Fig. 3). Notably, all three provide strong evidence of a phase transition. Below $T = 0.2$ K, pronounced kinks in all three ob-

servables are seen at a characteristic field, $H^* \approx 3.9$ T, that is almost temperature independent as it increases from 3.8 T at 0.05 K to 4.0 T at 0.17 K. As shown in Fig. 3A and

the inset of Fig. 3B, diamagnetic shielding and zero resistivity persist up to the superconducting critical field, further proving that this is a phase transition within the superconducting state. In contrast, field-dependent data for $H\parallel ab$ show no sign of such a phase transition (fig. S6) (17).

Using the values of T_c , H_{c2} [defined in $\chi_{ac}(H)$ at the onset in the same way as in the temperature sweeps], and H^* from our measurements, we show the superconducting phase diagrams of CeRh_2As_2 for out-of-plane and in-plane fields in Fig. 4, A and B, respectively. From these phase diagrams, the superconducting critical field can be extrapolated to $H_{c2}(0) \approx 14$ T for $H\parallel c$ and 1.9 T for $H\parallel ab$. For $H\parallel c$, two superconducting states appear, labeled as SC1 and SC2, separated by a line that intersects the strong kink in the $H_{c2}(T)$ curve in a multicritical point.

It is useful to estimate the upper critical fields with the Werthamer-Helfand-Hohenberg (WHH) formula $H_{\text{orb}} \approx 0.693T_c \left(-\frac{dH_{c2}}{dT}\right)_{T_c}$, which only uses parameters near T_c where Pauli paramagnetic pair-breaking effects are parametrically suppressed (23). Using the large experimental slopes $\left(-\frac{dH_{c2}}{dT}\right)_{T_c} = 97$ T/K for $H\parallel c$ and 45 T/K for $H\parallel ab$, this yields $H_{\text{orb}} \approx 17$ T and $H_{\text{orb}} \approx 8$ T, respectively. Their anisotropy of a factor of ≈ 2 reflects the anisotropy of the effective mass, because $H_{\text{orb}} \propto m^{*2}$ (24). The corresponding BCS coherence lengths $\xi = \sqrt{\Phi_0/2\pi H_{c2}(T=0)}$, where Φ_0 is the flux quantum, are accordingly small, lying below 100 Å. The H_{orb} estimates suggest that the upper critical field of SC2 along the c axis is not Pauli-paramagnetically suppressed. In contrast, we find that the superconducting state SC1 is strongly Pauli limited, with Pauli critical fields that are enhanced compared with the Clogston-Chandrasekhar limit of ≈ 0.5 T and 2.5 to 3 times larger for $H\parallel c$ than for $H\parallel ab$. This factor represents the scaling factor of the experimental critical field of SC1 for the two magnetic field directions.

The role of spin-orbit coupling

Our key results on the superconducting properties of CeRh_2As_2 can be summarized as follows.

1) A large anisotropy in the critical fields, with a c axis critical field (14 T) far exceeding the in-plane critical field (1.9 T). Indeed, $\mu_0 H_{c2}/T_c$ for c axis fields achieves the highest value thus far observed in Ce-based heavy-fermion superconductors.

2) A superconducting state SC1 from which a second c axis field-induced superconducting phase, SC2, appears.

3) The critical fields of SC1 are Pauli limited, in contrast to the critical field for SC2 and $H\parallel c$, which far exceeds the Pauli field.

4) The c axis Pauli field (~ 5 T) for SC1 is substantially larger than the in-plane Pauli field (1.9 T).

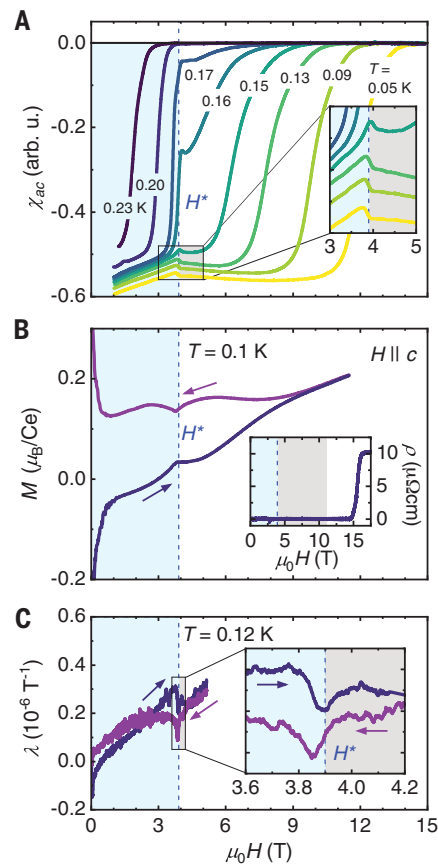


Fig. 3. Phase transition inside the superconducting state for $H\parallel c$. (A) Absolute value of the magnetic susceptibility χ_{ac} for different temperatures, as indicated. (Inset) Zoom on the transition at H^* . (B) Magnetization M at 0.1 K. (Inset) Resistivity at 0.1 K. (C) Magnetostriction at 0.12 K. (Inset) Zoom on the transition at H^* . The dashed line is a guide to the eye indicating the H^* transition at ≈ 3.9 T.

Our first finding, the large anisotropy in the critical fields and large c axis critical field, is reminiscent of the noncentrosymmetric heavy-fermion superconductors CeCoGe_3 , CeRhSi_3 , and CeIrSi_3 (25–29), whose low crystal symmetry allows Rashba spin-orbit coupling (29, 30). Owing to the broken inversion symmetry in these materials, even-parity (spin-singlet) and odd-parity (spin-triplet) superconducting states are not distinct and are, in general, mixed. These mixed states generically reveal no Pauli paramagnetic suppression for fields along the c axis, whereas they do for in-plane fields (29, 30). However, these materials exhibit two important differences with respect to CeRh_2As_2 : The first is that they do not exhibit multiple superconducting phases, and the second is that inversion symmetry is preserved in CeRh_2As_2 . These two differences lead to an explanation for our second observation, of superconducting states S1 and S2. Although CeRh_2As_2 is centro-

symmetric, it is locally noncentrosymmetric, with an inversion symmetry linking two noncentrosymmetric Ce-square lattices, each of which has a Rashba interaction. A key feature of the centrosymmetric structure is that even-parity (spin-singlet) and odd-parity (spin-triplet) Cooper pairs are not mixed, such that a phase transition between even- and odd-parity condensates can occur. We argue that this is the case in CeRh_2As_2 . Indeed, a conceptually similar situation has been considered in models of bilayer materials, where the interplay between an intralayer Rashba interaction and interlayer hopping can lead to a c axis field-driven transition between two superconducting phases (13–15), similar to that observed here. Below, we show that the structure of CeRh_2As_2 allows this bilayer physics to appear in a crystalline setting.

To illustrate the relevance of spin-orbit coupling to determining the key physics of CeRh_2As_2 in spite of the presence of global inversion symmetry, we develop a model taking into account the unusual features of its structure. In particular, because Ce $4f$ electrons are key to the heavy quasiparticle bands that give rise to superconductivity, we consider Wannier functions for these bands that are centered on the Ce sites. The Ce atoms sit at sites with a local C_{4v} symmetry, for which electronic states belong to CEF doublets of either Γ_6 or Γ_7 symmetry. A symmetry-based tight-binding Hamiltonian, which takes the same form for either two Γ_6 or Γ_7 doublets, is

$$\begin{aligned}
 H_N = & t_1 [\cos(k_x) + \cos(k_y)] - \mu + \\
 & \alpha_R \tau_z [\sin(k_x)\sigma_y - \sin(k_y)\sigma_x] + \\
 & t_{c,1} \tau_x \cos\left(\frac{k_z}{2}\right) \cos\left(\frac{k_x}{2}\right) \cos\left(\frac{k_y}{2}\right) + \\
 & t_{c,2} \tau_y \sin\left(\frac{k_z}{2}\right) \cos\left(\frac{k_x}{2}\right) \cos\left(\frac{k_y}{2}\right) + \\
 & \lambda \tau_z \sigma_z \sin k_z (\cos k_x - \cos k_y) \sin k_x \sin k_y
 \end{aligned} \quad (1)$$

Here, the σ_i Pauli matrices represent the two Kramer's spin-like degenerate states of the Γ_6 or Γ_7 doublets, and the τ_i Pauli matrices represent the two Ce site degrees of freedom in each unit cell. Given that these two Ce site degrees of freedom are related by inversion symmetry, the τ_z matrix is odd under inversion symmetry (this follows because this matrix changes sign when the two Ce sites are interchanged). Inspection of Eq. 1 shows that a Rashba-like spin-orbit interaction, denoted by the constant α_R , is allowed by symmetry, with the odd inversion symmetry compensated for by the τ_z operator. Equation 1 also reveals an additional Ising-like spin-orbit coupling term denoted by λ , with a $\tau_z \sigma_z$ dependence. This term will be much smaller than α_R because α_R

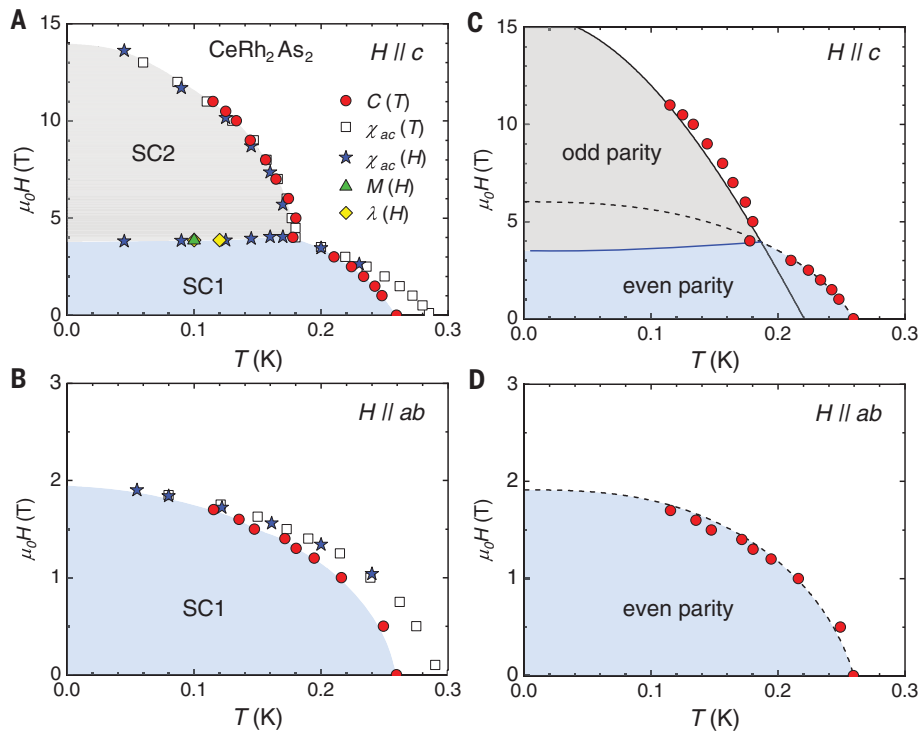


Fig. 4. Superconducting phase diagrams for CeRh₂As₂. (A) $H||c$ and (B) $H||ab$. Different symbols are from different experimental probes, as indicated in (A). (C) Fits to the upper critical fields for even-parity (dashed line) and odd-parity (solid line) states and a fit to the first-order phase boundary between an even- and odd-parity state (solid blue line). (D) Fit to the upper critical field for an even-parity state. For details of the fitting procedure, see (17).

originates from nearest neighbor ($a,0,0$)-type hoppings, whereas λ requires much longer range ($a,2a,c$)-type hoppings; for this reason, we set $\lambda = 0$ for our calculations on CeRh₂As₂. The two parameters $t_{c,i}$ correspond to c -axis ($a/2, a/2, c/2$) hoppings between the two Ce sublattice sites.

We now turn to the superconducting state. Density functional theory (DFT) reveals that the band structure for the conduction electrons is quasi-two dimensional, so it is natural to assume that the quasiparticle interactions that give rise to superconductivity originate in the two-dimensional square Ce layers, which consist of only Ce sites from the same sublattice. So, in terms of τ_i operators, the Cooper pairs can have only a τ_0 or a τ_z dependence. Formally, τ_0 (τ_z) describes Cooper pair wave functions that have the same (opposite) sign on the two Ce sublattice sites. For simplicity, we will assume that each sublattice prefers a spin-singlet s -wave Cooper pair. This is not essential for the arguments presented below, which rely on the τ_i structure of the Cooper pairs; the analysis also applies to a d -wave state such as those commonly found in tetragonal Ce materials. Below, we explicitly consider the even-parity gap function $\Delta_e = \Delta\tau_0$ and the odd-parity gap function $\Delta_o = \Delta\tau_z$. We note that similar gap func-

tions have been discussed in three-dimensional Cu₂Bi₂Se₃ (31), and Δ_o -type gap functions were originally proposed by P. W. Anderson as the generic form of odd-parity superconductivity in heavy-fermion materials (32). These results indicate that Δ_e - and Δ_o -type gap functions are stable solutions in general and not only in the quasi-two-dimensional limit considered here.

In (17), we carry out a detailed analysis of Eq. 1 on the superconducting state by projecting onto a pseudospin basis. This analysis yields four generic results that apply to all superconducting states described in the previous paragraph: (i) The pairing interactions for Δ_e and Δ_o have the same sign (both are attractive). (ii) Δ_e has a higher transition temperature than Δ_o in zero field. (iii) Δ_e is Pauli suppressed by a c axis field, whereas Δ_o is not (note the suppression of Δ_e by H_z is weaker than the usual paramagnetic suppression, i.e., the Pauli limit is enhanced). A c axis field will therefore induce a first-order phase transition from Δ_e to Δ_o . (iv) For in-plane fields, both Δ_e and Δ_o are Pauli suppressed. These results naturally account for observations 1 and 2 listed at the beginning of this section. We then use a simplified model to fit the data, with the results shown in Fig. 4, C and D. These fits account for observations 1 through

4 and suggest that the situation in CeRh₂As₂ is in close correspondence with that described in earlier theoretical work on a model for which, until now, there were no candidate materials (14, 15). Although the core results that we present here are experimental, and we do not claim that our simple model is the only possible explanation for our findings, it is notable that the model succeeds in accounting for all our key observations.

As a final point, we look at the multicritical point in the phase diagram for $H||c$. In general, thermodynamic considerations forbid that three second-order transition lines meet at a multicritical point (33, 34). However, the phase diagram as experimentally determined here for $H||c$ is thermodynamically possible if two second-order transition lines and one first-order transition line meet (34), and the model suggests that the first-order transition line is the one inside the superconducting state. Several experimental observations point to this scenario as well; an analysis of the slopes of the transition lines and their relation to the size of the specific heat jumps near the multicritical point is consistent with it [fig. S8 and discussion in (17)]. Furthermore, the dip in the magnetostriction at H^* corresponds to a steplike change of the sample length and shows hysteresis of ~ 0.04 T (Fig. 3C). However, these experimental features are extremely small and not confirmed by any other probe, so the experimental evidence for the transition within the superconducting state being first order should not yet be regarded as conclusive.

At present, we cannot exclude the possibility that the phase diagram including the normal state is more complicated. The putative ordered state below $T_0 \approx 0.4$ K also seems to be suppressed near $H \approx 4$ T (Fig. 2B), and the transition line might join the multicritical point as a fourth transition line. Thermodynamically, this would allow the transition within the superconducting state to be second order, and it would place further constraints on the slopes of the lines and the ratios of the specific heat jumps. More generally, it is possible that the change of the superconducting state is influenced by a change in the normal state when the order below T_0 is suppressed. A more detailed study of the specific heat and the magnetocaloric effect would likely be able to resolve the issue.

It is informative to compare our findings with recent developments in UTe₂ (35, 36), wherein multiphase superconductivity has been established in the H - T phase diagram under the application of hydrostatic pressure (37) and a splitting of T_c has been reported at ambient pressure (38). A substantial body of theoretical work has been done on UTe₂ (39–44). The prevailing opinion is that the relevant phases are all triplet, and spin fluctuations are thought

to be the main driver of the relevant physics. Spin fluctuations are a possible mechanism for superconductivity in CeRh₂As₂ as well. Typically, these fluctuations stabilize either even- or odd-parity states, but not both. However, in the unusual electronic environment of CeRh₂As₂, Rashba spin-orbit coupling allows both even- and odd-parity states to be stabilized by the same underlying pairing interaction, opening up the possibility of an even-to-odd parity phase transition.

Outlook

Many open questions remain about the precise nature of the superconducting mechanism in CeRh₂As₂, including the possibility that the superconductivity in zero applied magnetic field condenses from a normal state that already includes unidentified order. Like its superconductivity, that “hidden” order is probably rooted in the unusual Ce environment. CeRh₂As₂ therefore highlights the importance of local symmetry breaking not just for superconductivity but for metallic correlated electronic order as well.

REFERENCES AND NOTES

- A. J. Leggett, *Rev. Mod. Phys.* **47**, 331–414 (1975).
- M. Sigrist, K. Ueda, *Rev. Mod. Phys.* **63**, 239–311 (1991).
- R. A. Fisher *et al.*, *Phys. Rev. Lett.* **62**, 1411–1414 (1989).
- S. Adenwalla *et al.*, *Phys. Rev. Lett.* **65**, 2298–2301 (1990).
- R. Joynt, L. Taillefer, *Rev. Mod. Phys.* **74**, 235–294 (2002).
- M. Shimozawa, S. K. Goh, T. Shibauchi, Y. Matsuda, *Rep. Prog. Phys.* **79**, 074503 (2016).
- S. L. Wu *et al.*, *Nat. Commun.* **8**, 1919 (2017).
- K. Gottlieb *et al.*, *Science* **362**, 1271–1275 (2018).
- H. Ishikawa *et al.*, *Inorg. Chem.* **58**, 12888–12894 (2019).
- X. Zhang, Q. Liu, J.-W. Luo, A. J. Freeman, A. Zunger, *Nat. Phys.* **10**, 387–393 (2014).
- L. Yuan *et al.*, *Nat. Commun.* **10**, 906 (2019).
- M. H. Fischer, F. Loder, M. Sigrist, *Phys. Rev. B* **84**, 184533 (2011).
- M. Sigrist *et al.*, *J. Phys. Soc. Jpn.* **83**, 061014 (2014).
- T. Yoshida, M. Sigrist, Y. Yanase, *Phys. Rev. B* **86**, 134514 (2012).
- D. Maruyama, M. Sigrist, Y. Yanase, *J. Phys. Soc. Jpn.* **81**, 034702 (2012).
- R. Madar, P. Chaudouet, J. P. Senateur, S. Zemni, D. Tranqui, *J. Less Common Met.* **133**, 303–311 (1987).
- Materials and methods are available as supplementary materials.
- A. Steppke *et al.*, *Science* **339**, 933–936 (2013).
- H. S. Jeevan, C. Geibel, Z. Hossain, *Phys. Rev. B* **73**, 020407 (2006).
- E. Hassinger *et al.*, *Phys. Rev. B* **77**, 115117 (2008).
- M. D. Bachmann *et al.*, *Science* **366**, 221–226 (2019).
- J. F. Landaeta *et al.*, *Phys. Rev. B* **97**, 104513 (2018).
- N. R. Werthamer, E. Helfand, P. C. Hohenberg, *Phys. Rev.* **147**, 295–302 (1966).
- J. P. Brison *et al.*, *Physica C Supercond.* **250**, 128–138 (1995).
- M. A. Méasson *et al.*, *Physica C Supercond.* **470**, S536–S538 (2010).
- N. Kimura *et al.*, *Phys. Rev. Lett.* **95**, 247004 (2005).
- I. Sugitani *et al.*, *J. Phys. Soc. Jpn.* **75**, 043703 (2006).
- N. Kimura, K. Ito, H. Aoki, S. Uji, T. Terashima, *Phys. Rev. Lett.* **98**, 197001 (2007).
- E. Bauer, M. Sigrist, Eds., *Non-Centrosymmetric Superconductors: Introduction and Overview*, vol. 847 of *Lecture Notes in Physics* (Springer-Verlag, 2012).
- M. Smidman, M. B. Salamon, H. Q. Yuan, D. F. Agterberg, *Rep. Prog. Phys.* **80**, 036501 (2017).
- L. Fu, E. Berg, *Phys. Rev. Lett.* **105**, 097001 (2010).
- P. W. Anderson, *Phys. Rev. B* **32**, 499 (1985).
- A. J. Leggett, *Prog. Theor. Phys.* **51**, 1275–1277 (1974).
- S. K. Yip, T. Li, P. Kumar, *Phys. Rev. B* **43**, 2742–2747 (1991).
- S. Ran *et al.*, *Science* **365**, 684–687 (2019).
- D. Aoki, K. Ishida, J. Flouquet, *J. Phys. Soc. Jpn.* **88**, 022001 (2019).
- D. Aoki *et al.*, *J. Phys. Soc. Jpn.* **89**, 053705 (2020).
- I. M. Hayes *et al.*, *Science* **373**, 797–801 (2021).
- K. Machida, *J. Phys. Soc. Jpn.* **89**, 065001 (2020).
- S. Sundar *et al.*, *Phys. Rev. B* **100**, 140502 (2019).
- Y. Xu, Y. Sheng, Y.-F. Yang, *Phys. Rev. Lett.* **123**, 217002 (2019).
- J. Ishizuka, S. Sumita, A. Daido, Y. Yanase, *Phys. Rev. Lett.* **123**, 217001 (2019).
- J. Ishizuka, Y. Yanase, *Phys. Rev. B* **103**, 094504 (2021).
- T. Shishidou, H. G. Suh, P. M. R. Brydon, M. Weinert, D. F. Agterberg, *Phys. Rev. B* **103**, 104504 (2021).
- S. Khim *et al.*, Raw Data for “Field-induced transition within the superconducting state of CeRh₂As₂,” Max Planck Society (2021); <https://dx.doi.org/10.17617/3.72>.

ACKNOWLEDGMENTS

We strongly appreciated discussions with D. Cavanagh, O. Erten, M. Fischer, J. S. Kim, D. Möckli, A. Ramirez, B. Schmidt, M. Sigrist, P. Thalmeier, H.-U. Desgranges, H. Rosner, K. Ishida, Y. Yanase, G. Zwicker, and S. Wirth. We thank M. König, U. Burkhardt, M. Eckert, and S. Kostmann for EDX measurements. **Funding:** We acknowledge funding from the Physics of Quantum Materials department and the research group “Physics of Unconventional Metals and Superconductors (PUMAS)” of the Max Planck Society. C.G. and E.H. acknowledge support from the German Science Foundation (DFG) through grant GE 602/4-1 Fermi-NEST. P.M.R.B. was supported by the Marsden Fund Council from Government funding, managed by Royal Society Te Apārangi. R.K. is supported by the DFG through project no. KU 3287/1-1. D.F.A. was supported by the US Department of Energy, Office of Basic Energy Sciences, Division of Materials Sciences and Engineering, under award DE-SC0021971. The research environment in Dresden benefits from the DFG Excellence Cluster Complexity and Topology in Quantum Matter (ct.qmat). **Author contributions:** S.K. and C.G. grew the single crystals. S.K., J.F.L., J.B., N.B., M.B., D.H., R.K., U.S., and E.H. performed the measurements and data analysis. R.C.-G. conducted single-crystal diffraction measurements. P.M.R.B. and D.F.A. constructed the theoretical model. S.K., J.F.L., M.B., D.H., U.S., A.P.M., D.F.A., C.G., and E.H. interpreted the data. All authors were involved in designing the experiment and writing the manuscript. **Competing interests:** The authors declare that they have no competing interests. **Data and materials availability:** The data presented in this manuscript are available online at the Open Research Data Repository of the Max Planck Society (45).

SUPPLEMENTARY MATERIALS

science.sciencemag.org/content/373/6558/1012/suppl/DC1
Materials and Methods
Supplementary Text
Figs. S1 to S8
Tables S1 and S2
References (46–62)

11 September 2020; accepted 23 July 2021
10.1126/science.abe7518

Field-induced transition within the superconducting state of CeRhAs

S. KhimJ. F. LandaetaJ. BandaN. BannorM. BrandoP. M. R. BrydonD. HafnerR. K uchlerR. Cardoso-GilU. StockertA. P. MackenzieD. F. AgterbergC. GeibelE. Hassinger

Science, 373 (6558), • DOI: 10.1126/science.abe7518

Not your usual superconductor

Most superconductors have only one superconducting phase. Khim *et al.* measured the magnetic susceptibility of the heavy fermion material CeRhAs to reveal the presence of two distinct superconducting phases, one of which emerges from the other when an external magnetic field is applied (see the Perspective by Pourret and Knebel). The researchers ascribe the unusual properties of CeRhAs to its crystal structure, which is globally centrosymmetric but consists of noncentrosymmetric layers. —JS

View the article online

<https://www.science.org/doi/10.1126/science.abe7518>

Permissions

<https://www.science.org/help/reprints-and-permissions>

Use of think article is subject to the [Terms of service](#)

Science (ISSN) is published by the American Association for the Advancement of Science. 1200 New York Avenue NW, Washington, DC 20005. The title *Science* is a registered trademark of AAAS.

Copyright © 2021 The Authors, some rights reserved; exclusive licensee American Association for the Advancement of Science. No claim to original U.S. Government Works